Preliminary Study on Macro-Cell Corrosion of Steel Bars in Seawater Mixed Concrete with Various Interfacial Transition Zones

Tarek Uddin Mohammed[1], Md. Aktaruzzaman Rony*[1], Labiba Amin Parisa[1], Maliha Mahjabin[1], Mozidun Nahar Lorin[1], Md. Zawad Rafid[1]

[1] Islamic University of Technology, Dhaka, Bangladesh
aktaruzzaman@iut-dhaka.edu

Abstract. This study evaluated the corrosion of steel in seawater-mixed concrete with different interfacial transition zones (ITZs) by measuring different corrosion parameters. The ITZs around the steel bars were intentionally varied by applying cement paste coating around the steel bars, which had various water to cement ratios (W/Cs = 0.3, 0.5, and 0.7). Four cases made with slag cement (68% slag) were investigated, including a control case in which no coating was used. To assess macro-cell corrosion current density prism specimens have been made using segmented steel bars. From the casting of the specimens, until they were 30 days old, the current flow was recorded by electrically connecting the segmented steel bars outside the specimens with a data logger. Monitoring of the half-cell potentials throughout steel bars was carried out and measurements of the macro-cell corrosion were completed. Regardless of the specific cases studied, macro-cell corrosion exhibited a consistent trend of decrease. Steel bars having different cement paste coating with low W/Cs improved the ITZs, creating a dense steel-concrete interface that acted as a barrier against chloride ions permeability. However, a cement paste coating with high W/Cs showed more depth of corrosion compared to the control case than the case without coating because of the weak steel-concrete interface.

Keywords: *Interfacial Transition Zones, Macro-cell Corrosion, Half-cell Potential, Depth of Corrosion*

1 Introduction

Concrete is the most widely used modern building material due to its durability, strength, and versatility in construction [1]. In each year, 30 billion tonnes of concrete is used worldwide [2]. Corrosion of the steel rebar will result from several components, including the diffusion of aggressive agents, such as the chloride ions, and the reduced alkalinity of the passivation layer around the steel bar caused by carbonation [3]. Natural carbonation and external chloride ion ingress into the concrete are the main factors causing rebar corrosion [4]. Concrete structures can experience early deterioration due

Md.K. Miah et al. (eds.), *Proceedings of the 1st International Conference on Recent Innovation in Civil Engineering and Architecture for Sustainable Development (IICASD 2024)*, Advances in Engineering Research 260,
https://doi.org/10.2991/978-94-6463-672-7_16

to steel corrosion in marine and high-level salty environments, resulting in reduced durability performance [5]. To address this issue and minimize environmental impacts, it is necessary to increase concrete's service life by identifying and understanding the causes of corrosion. Chloride attack is particularly harmful, as chloride ions over a threshold level destroy the passivation film, which protects steel bars from corrosion in concrete [6, 7]. When the concentration of chloride on the surface of the steel exceeds a certain threshold level (the equivalent of about cement mass of 0.4% or 1.2 kg/m^3 of concrete samples), [8], pitting corrosion begins. Corrosion products are formed by the activation of the corrosive process, which further expands in volume and produces cracks. It ultimately causes the collapse of the structure. [9]. A corrosion cell may form due to potential differences either within a single rebar or between multiple rebars. This leads to the formation of the local anode and a local cathode [10]. The corrosion process is known as macro-cell corrosion when the anode and cathode are clearly segregated. The macro-cell corrosion becomes faster for the more significant potential difference [11].

In coastal regions, structures such as marine infrastructures, seaports, and tunnels are particularly vulnerable to corrosion due to the presence of seawater. This presents a challenge in countries like Bangladesh, where numerous large-scale projects are underway near the coast. Given the global shortage of fresh water, using it in concrete mixtures is unsustainable. Worldwide, about 2.2 billion people lack access to safe drinking water [12]. As an alternative, seawater can be used in concrete production. At the interfacial transition zones, the formation of voids occurs and causes corrosion, according to numerous studies of research that have been carried out on the corrosion of steel bars in sea-water mixed concrete systems [13–15]. When compared to the identical thing that happens with tap water, it will also result in the production of corrosion pits that are considerably deeper [4]. Research on the corrosion of steel in concrete has explored factors like temperature, water-cement ratios [16], corrosion inhibitors [17], the effect of bar types on corrosion [18, 19], the effect of different water-reducing chemical admixtures [20], etc. Based on the previous studies, it is clearly understood that in marine exposure, the steel-concrete interface is a crucial issue to begin corrosion over the steel bars in concrete [4]. The presence of a thin and dense hydration layer around the voids located at ITZ around steel bars in concrete protects the steel bars from corrosion even after exposure to seawater for 15 years [21].

More research related to the interface between concrete and steel is required, and research on the early stage of corrosion monitoring using seawater is very limited. This research is planned to understand this pressing need. By creating different ITZ compositions, this research seeks to determine which one can best obstruct the penetration of chloride ions at the early stage of casting, thus improving the concrete’s resistance to corrosion. Within the scope of seawater-mixed concrete, the purpose of this research is to get an understanding of the progress of macro-cell corrosion with varying ITZs around the steel bars from the time of casting over the steel bars.

2 Methodology

2.1 Material Properties

CEM Type III-B cement, as specified in BDS-EN-197-1-2010, was used to make the specimens. The slag content in this cement was 68% of the cement mass. Also, CEM Type III-B cement was used to coat the cement paste around the steel bars. The specific gravity of cement was 2.90 as per ASTM C188. The slump test value of the concrete was 125 mm. Stone chips and natural river sand were used as coarse and fine aggregates. The coarse aggregate's nominal maximum size was 20 mm. The physical properties of coarse and fine aggregates, as well as seawater, are summarized in Table 1 and Table 2.

The diameter of the reinforcement steel bars was 10 mm. The chemical composition of steel bars is carbon (0.22%), silicon (0.2%), manganese (0.65%), phosphorous (0.031%), sulfur (0.031%), and iron (98.868%). The minimum yield strength of the steel bar was 500 MPa, and it was made in accordance with ASTM A706 standards. Segmented steel bars (135 mm on both sides and 50 mm in the middle) were used to monitor macro-cell corrosion current density.

The segmented steel bars were isolated in specimens, and electrical connections were provided using electrical wires from the outside connected to the data logger. In addition to the segmented steel bars, an isolated continuous steel bar was also provided at the same depth adjacent to the segmented bars to prevent the specimens from collapsing. Fresh seawater from the Bay of Bengal was collected and used to prepare the concrete mixture.

Table 1. Coarse and fine aggregate's properties

Types of Aggregate	Coarse Aggregate	Fine Aggregate	Test Method
Specific gravity	2.66	2.57	ASTM C127
Absorption Capacity	0.91	2.59	ASTM C127
Abrasion value (%)	15.3	-	ASTM C131
Fineness Modulus (FM)	6.55	2.44	ASTM C136
Unit weight (kg/m^3)	1575	1517	ASTM C29

Table 2. Seawater's physical and chemical composition

pH	Na	K	Ca	Mg	Cl	SO_4	CO_3
				(ppm)			
7.8	10750	400	415	1303	18954	2407	143

2.2 Cases Investigated

Four different cases were investigated with prism specimens sized 100 mm in width, 100 mm length and 400 mm in length made with three-segmented and one continuous steel bar of diameter 10 mm. Also, 100 mm diameter and 200 mm height cylinder specimens were prepared to measure compressive strength of concrete. The cases investigated are described in Table 3. Water to cement ratio (W/C) was 0.45. In total, four prism specimens and 12 cylinders were prepared. Table 4 illustrates the mixture proportions of concrete. Sea water was used in mixing concrete with a chloride concentration of 12.7% of the cement mass. It was calculated based on the concentration of chloride in seawater. For the cement coating, different water-cement ratios for different cases were used.

Table 3. Cases investigated

Cases	Coating of segmented middle and continuous left bar (W/C)	Coating of segmented edge and continuous right bar (W/C)
(Controlled) 1	No Coating	No Coating
2	0.3	0.3
3	0.5	0.3
4	0.7	0.3

Table 4. Mixture Proportions of Concrete

W/C	S/A	Cement	Seawater	Fine Aggregate	Coarse Aggregate
		(kg/m^3)			
0.45	0.44	340	153	806	1058

2.3 Details of Specimens

The steel bars underwent a cleansing process utilizing a 10% solution of diammonium hydrogen citrate. The continuous steel bar measures 340 mm in length. Three distinct segmented bars were utilized for the measurement of macro-cell corrosion current: two bars measuring 135 mm each and a central bar measuring 50 mm. The wires were joined through the process of soldering with steel bars. Fig. 1 illustrates the specifics of the prism specimens. The segmented steel bars were electrically connected from outside the specimens by electrical wires. To provide electrical isolation inside the specimens, the segmented steel bars were connected by epoxy. Prior to the making of the specimens, a cement paste coating was thoroughly applied to the steel bars, each demonstrating separate water-cement ratios (W/Cs) specific for various cases. After coating, the coated steel bars were cured in a moist condition for 24 hours. In Fig. 2, demonstration of the connections that are made between coated steel bars and wires connecting

steel bars. By placing a resistor with a resistance of 100 ohms, the voltage drop was measured.

A data logger (TDS 150) recorded the voltage drops at 60 sec intervals. The connection of the rebars with the data logger is shown in Fig. 3. As the specimens were created using seawater in concrete mixing, macro-cell corrosion monitoring was started during the placement of concrete in the mold. The specimens had been connected to the data logger prior to casting, and the voltage drops were promptly measured from the casting to assess macro-cell corrosion current. The thickness of the concrete cover measured 20 mm. Subsequent to the casting process, the prism specimens underwent a curing period of thirty days, covered in wet jute bags that were thoroughly sealed with polythene to maintain a constantly moist environment for the specimens.

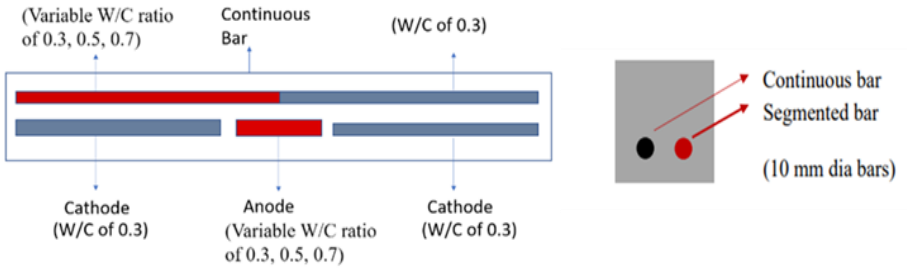

Fig. 1. Details of prism specimens.

Fig. 2. The connection of the coated steel bars with wires.

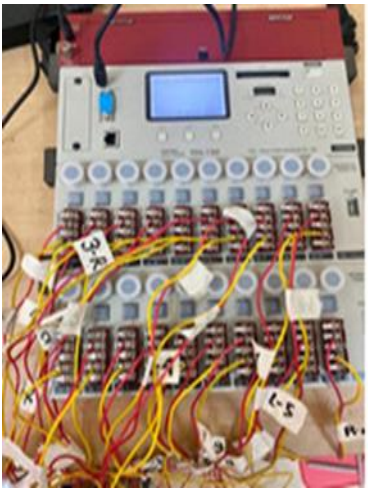


Fig. 3. Connection of rebars with data logger.

2.4 Methods of Evaluation

Ultrasonic Pulse Velocity (UPV). The ultrasonic pulse velocity (UPV) is a non-destructive method for assessing concrete's homogeneity, quality, cracks, and internal flaws. UPV was measured according to ASTM C597. The quality of concrete can be evaluated based on the guidelines summarized in Table 5.

Table 5. Concrete quality with respect to pulse velocity (BIS 13311-92-Part-I).

UPV	Concrete Quality
>4500 m/s	Excellent
3500-4500 m/s	Good
3000-3500 m/s	Medium
<3000 m/s	Very low

Compressive Strength Test. The compressive strength of concrete was evaluated at 7, 28, 56, and 90 days as per ASTM C39.

Macrocell Corrosion. Segmented steel bars have been used to assess macro-cell corrosion current density, with steel bars those being externally connected via a data logger. A resistor of 100 Ω has been integrated into the circuit to assess the voltage drop across two segmented steel bars. The investigation continued from the moment of specimen casting to track the current flow immediately upon the interaction of seawater-mixed concrete with the steel bars. The potential declines were documented at a predetermined interval of one minute interval. The current can be determined by analyzing the voltage drop across a resistance that remains constant, using equation (1).

$$I = \frac{V}{R} \quad (1)$$

where I = Current (A), V = Voltage drop (V), R = Resistance (100 Ω).
The macro-cell corrosion current density was determined by utilizing equation (2).

$$I_{mac} = \frac{I}{A} \times 10^6 \quad (2)$$

where A=surface area (segmented steel) (cm^2), I= current (A), and I_{mac} = macro-cell corrosion current density ($\mu A/cm^2$).

Using equation (3), the depth of the corrosion that had occurred across the steel bars were determined [22]:

$$D = 0.0116 \times I_{avg} \times t \quad (3)$$

where D= depth of corrosion (mm), I_{avg} = macro-cell corrosion current density ($\mu A/cm^2$), and t =time (years) . I_{avg} was determined by evaluating the area beneath the curve of the complete experiment, subsequently divided by the duration of exposure.

Half-Cell Potential. The measurement of the half-cell potential (HCP) was conducted utilizing an Ag/AgCl half-cell. Half-cell potentials of segmented steel bars were later evaluated after a period of time that was first dedicated to the continuous monitoring of macro-cell corrosion currents. The steel segments underwent electrical isolation throughout the HCP measurement process. The assessment of corrosion probability was conducted in accordance with ASTM C876 guidelines, utilizing the half-cell potential (Ag/AgCl) values as detailed in Table 6.

Table 6. Ag/AgCl half-cell potential with corresponding probability of corrosion (ASTM C876).

Potential mV vs. Ag/AgCl	Corrosion Probability (%)
More -ve than -255	> 90% (active)
Between –255 to -105	Uncertain
More +ve than -105	< 10% (passive)

3 Results And Discussions

3.1 Ultrasonic Pulse Velocity (UPV)

Fig. 4 shows the UPV of concrete at 7, 28, 56, and 90 days. Due to continuous hydration over time, the UPV increases with time. Irrespective of the age of the specimens, the UPV is over 3500 m/s, and the results specify that the quality of concrete is good. The UPV values are in the medium range of the concrete and very close to excellent because of the dense microstructure of the slag cement [23].

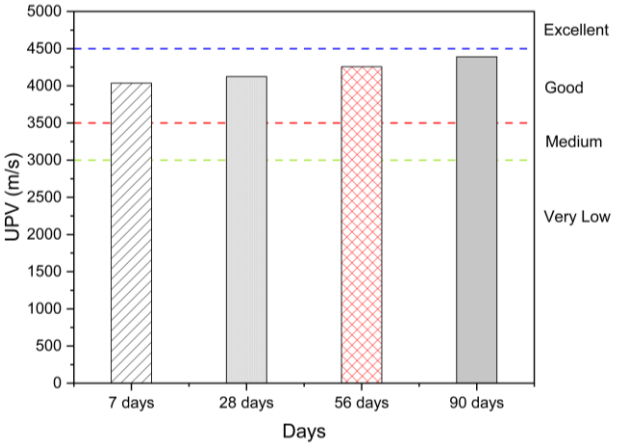

Fig. 4. Variation of UPV at 7, 28, 56, and 90 days.

3.2 Compressive Strength

The compressive strengths of concrete were evaluated at 7, 28, 56, and 90 days, which are shown in Fig. 5. CEM Type III B cement, which contains 68% slag, was used. As a result, significant development of strength was observed by 28 days. It was found that at 7 days, more than 70% of the strength of 28 days was developed. The observed results align with previous studies, where seawater-mixed concrete exhibited earlier strength gain. However, no significant long-term difference in compressive strength was observed. [24]. It is important to note that seawater speeds up the early-stage hydration of cement, leading to increased concrete strength due to higher density. This occurs because the chlorides in seawater react with calcium hydroxide (CH), a byproduct of cement hydration, to form calcium chloride ($CaCl_2$) [25].

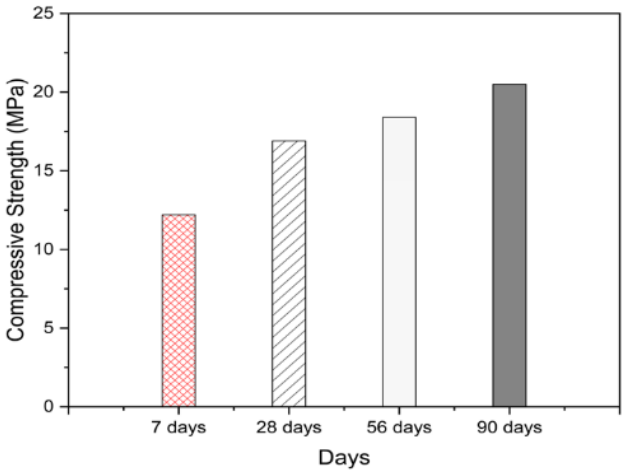

Fig. 5. Compressive strength of seawater mixed concrete.

3.3 Macro-cell Corrosion Current Density (I_{mac})

Data associated with macro-cell corrosion current density, observed over a duration of 30 days, is presented in Fig. 6. Upon the initial interaction of seawater-mixed concrete with a steel bar, there is an observable increase in the macro-cell corrosion current density; nevertheless, this phenomenon diminishes over time. A considerable decrease in the macro-cell corrosion current density was seen throughout the duration of time in situations where the coating had a low W/C ratio, particularly for W/C= 0.3.

The same was also observed for the case without coating. However, in the case of cement paste coating with high W/C ratios of 0.5 and 0.7, macro-cell corrosion with a lower current level is continuing. The results indicate that macro-cell corrosion becomes significant in the case of a weaker/porous steel-concrete interface. For instance, it is most likely that in the case of cement paste coating of steel bars with a high W/C ratio, many voids will be created in the ITZ, which will help to continue the corrosion rate over time.

To quantitatively assess microcell corrosion current density, the areas beneath the macro-cell corrosion current density curves illustrated in Fig. 6 were computed, reflecting the extent of corrosion depth.

The findings are represented in Fig. 7. It is essential to recognize that the real corrosion depth might be much larger (varying from between four and eight times more) than the estimated depth based simply on corrosion current data, as mentioned in the mentioned reference [22]. The findings reveal that the most severe corrosion of steel bars incorporated into concrete occurred within the interfacial transition zone, which had its highest porosity. The severity of corrosion corresponded with the pattern of macro-cell corrosion current density and exhibited an increase together with higher water-to-cement ratios.

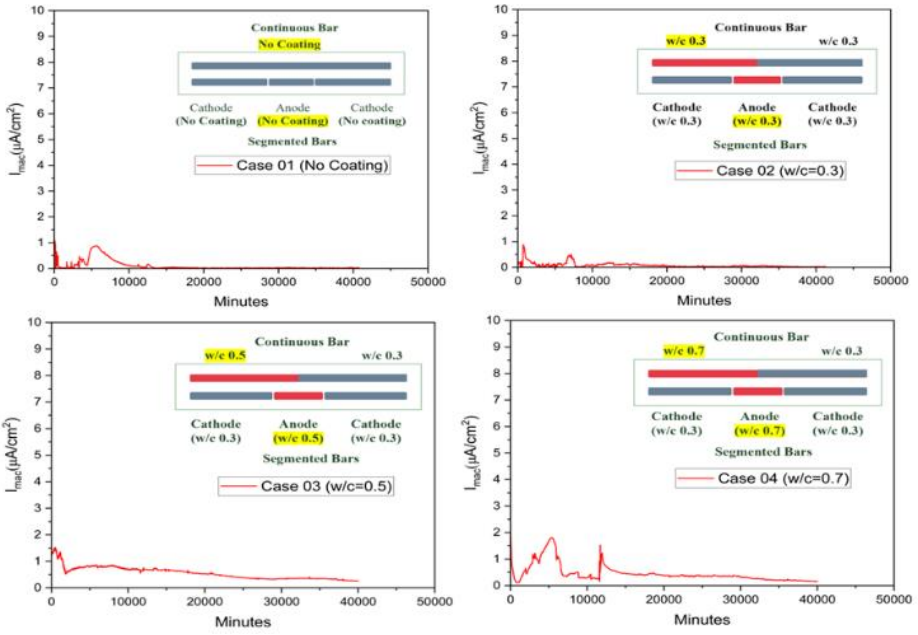

Fig. 6. Macro-cell corrosion current density.

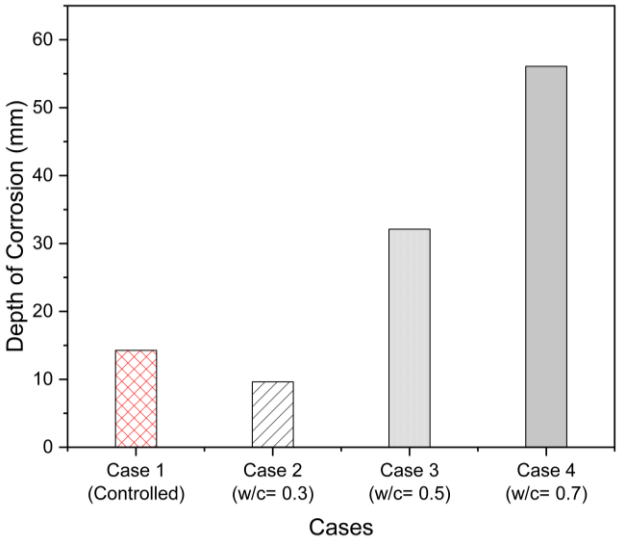

Fig. 7. Depth of corrosion.

3.4 Half Cell Potential (HCP)

After detaching the prism specimens from the data logger, half-cell potential was measured at 60, 74, and 95 days. This time, the specimens were fully submerged in seawater, and the temperature was controlled at 40 degrees Celsius. The results are shown in Fig. 8. Half-cell potential measurements confirmed that the segmented middle bar is acting as the anode due to its lower potential compared to the right and left bars. This suggests the formation of a weaker interface at the middle bar, promoting its corrosion activity, while denser interfaces formed on the right and left bars, acting as cathodes. It is clear that on day 60, half-cell potential of case 2 (W/C =0.3) is the lowest negative potential (less negative than -200 mV), which means it has the least probability of corrosion. Oppositely, case 4 (W/C =0.7) has the highest negative potential (less than -350 mV), which means it has the highest probability of corrosion. However, the controlled case shows lesser potential than a coated bar with a high W/C ratio. Although the controlled case might start with higher negative values indicating susceptibility to corrosion, if it shows a slower decline over time compared to cases with higher w/c ratios, it may still demonstrate better overall corrosion resistance. Both graphs demonstrated that higher W/C ratios accelerate the corrosion initiation, with the segmented middle showing a slightly greater decline in HCP values, indicating a higher susceptibility to corrosion.

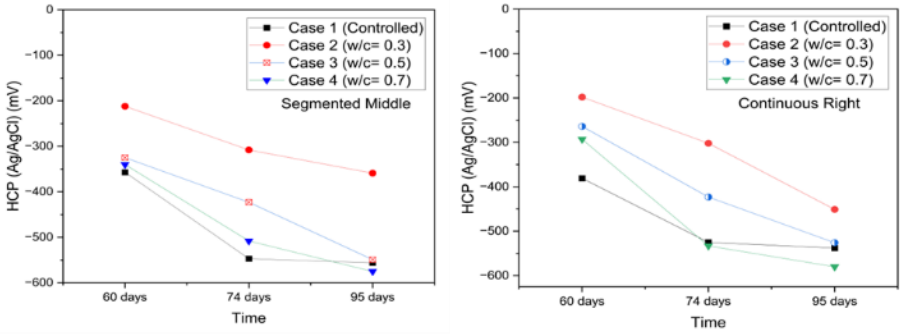

Fig. 8. Half-cell potential.

4 Conclusions

In accordance with the findings from this study, consequent conclusions were drawn regarding the formation of macro-cell corrosion in concrete mixed with seawater:

1. The interfacial transition zones surrounding steel bars significantly influence the progression of macro-cell corrosion as time goes on. Steel bars covered in cement paste which has a low water-to-cement ratio contribute to the reduction of macro-cell corrosion over time by establishing a dense micro-structure surrounding the steel bar, even in the presence of higher chloride levels.

2. Immediately after the casting, a peak of macro-cell corrosion has been found irrespective of coated and non-coated steel bars; the macro-cell corrosion current density, on the other hand, decreased throughout the period of time.
3. Macrocell corrosion current density increases positively and half-cell potential increases negatively with the increase in porosity of the ITZ.

Acknowledgments. The authors would like to convey their sincere gratitude and deep appreciation to the authority of the Islamic University of Technology (IUT) for their invaluable support in facilitating this study. We express our sincere appreciation for the assistance provided by Crown Cement PLC in supplying with cement and slag.

Disclosure of Interests. The authors declare no conflicts of interest that relate to the content of this article.

References

1. Mehta, P.K.: Concrete: microstructure, properties, and materials. McGraw-Hill, New York (2014)
2. Mack, Y.L., Oliveira, L.S., John, V.M.: Concrete Water Footprint Assessment Methodologies. Key Eng. Mater. 668, 247–254 (2015). https://doi.org/10.4028/www.scientific.net/KEM.668.247.
3. Song, G., Shayan, A.: Corrosion of steel in concrete: causes, detection and prediction: a state-of-the-art review. Presented at the July 1 (1998)
4. Mohammed, T.U., Hidennori, H., Toru, Y.: Performance of seawater-mixed concrete in the tidal environment. Cem. Concr. Res. 34, 593–601 (2004). https://doi.org/10.1016/j.cemconres.2003.09.020.
5. Alexander, M.: Service life design and modelling of concrete structures – background, developments, and implementation. Rev. ALCONPAT. 8, 224 (2018). https://doi.org/10.21041/ra.v8i3.325.
6. Bui, H.T., Maekawa, K., Tan, K.H.: Microcell and macrocell corrosion of steel bars in reinforced concrete slabs under different corrosive environments and cathode/anode configurations. Cem. Concr. Compos. 138, 104989 (2023). https://doi.org/10.1016/j.cemconcomp.2023.104989.
7. Dhir, R.K., McCarthy, M.J., Newlands, M.D.: Concrete for extreme conditions: proceedings of the international conference held at the university of Dundee, Scotland, UK on 9-11 September 2002. Presented at the , London (2002)
8. Brenna, A., Bolzoni, F., Beretta, S., Ormellese, M.: Long-term chloride-induced corrosion monitoring of reinforced concrete coated with commercial polymer-modified mortar and polymeric coatings. Constr. Build. Mater. 48, 734–744 (2013). https://doi.org/10.1016/j.conbuildmat.2013.07.099.
9. Aguirre-Guerrero, A.M., Robayo-Salazar, R.A., de Gutiérrez, R.M.: A novel geopolymer application: Coatings to protect reinforced concrete against corrosion. Appl. Clay Sci. 135, 437–446 (2017). https://doi.org/10.1016/j.clay.2016.10.029.
10. Elsener, B.: Macrocell corrosion of steel in concrete – implications for corrosion monitoring. Cem. Concr. Compos. 24, 65–72 (2002). https://doi.org/10.1016/S0958-9465(01)00027-0.
11. Wang, J., Wang, Q., Zhao, Y., Li, P., Ji, T., Zou, G., Qiao, Y., Zhou, Z., Wang, G., Song, D.: Research Progress of Macrocell Corrosion of Steel Rebar in Concrete. Coatings. 13, 853 (2023). https://doi.org/10.3390/coatings13050853.

12. UN News: Billions globally lack 'water, sanitation and hygiene', new UN report spells out | UN News, https://news.un.org/en/story/2019/06/1040701, last accessed 2024/10/01.
13. Mohammed, T. U., Rahman, M., Sabbir, A., Hasan, M.M., Mamun, A. A.: Chloride ingress and macro-cell corrosion of steel in concrete made with recycled brick aggregate. Front. Struct. Civ. Eng. 15, 1358–1371 (2021). https://doi.org/10.1007/s11709-021-0769-x.
14. Saumik, A.H., Zaman, R., Khan, M.S.H., Rony, M.A.: Control of Macro-Cell and Micro-Cell Corrosion of Steel In Cracked Concrete, http://103.82.172.44:8080/xmlui/handle/123456789/2130, (2023)
15. Mohammed, T.U., Hamada, H., Yamaji, T.: Concrete after 30 years of exposure—Part II: Chloride Ingress and Corrosion of Steel Bars. Mater. J. **101**, 13–18 (2004)
16. Ahmed, A.A., Shakouri, M., Trejo, D., Pavan Vaddey, N.: Effect of curing temperature and water-to-cement ratio on corrosion of steel in calcium aluminate cement concrete. Constr. Build. Mater. 350, 128875 (2022). https://doi.org/10.1016/j.conbuildmat.2022.128875.
17. Kokalj, A.: Corrosion inhibitors: physisorbed or chemisorbed? Corros. Sci. 196, 109939 (2022). https://doi.org/10.1016/j.corsci.2021.109939.
18. Mohammed, T. U., Otsuki, N., Hisada, M., Shibata, T.: Effect of Crack Width and Bar Types on Corrosionof Steel in Concrete. J. Mater. Civ. Eng. - J MATER Civ. ENG. **13**, (2001). https://doi.org/10.1061/(ASCE)0899-1561(2001)13:3(194).
19. Mi, Z., Chun, Q., Jin, H., Zhang, C., Shi, J.: Research on bond-slip behavior of corroded square rebar-concrete in historical reinforced concrete buildings. Case Stud. Constr. Mater. 21, e03686 (2024). https://doi.org/10.1016/j.cscm.2024.e03686.
20. Mohammed, T.U., T., F., Yamaji, T., Hamada, H.: Long-term Durability of concrete made with different water reducing chemical admixtures under marine environment. Presented at the Challenges of Concrete Construction , University of Dundee, Scotland January (2002). https://doi.org/10.1680/cfec.31784.
21. Mohammed, T.U., Yamaji, T., Hamada, H.: Microstructures and Interfaces in Concrete after 15 Years of Exposure in Tidal Environment. ACI Mater. J. **99**, (2002). https://doi.org/10.14359/12217.
22. González, J.A., Andrade, C., Alonso, C., Feliu, S.: Comparison of rates of general corrosion and maximum pitting penetration on concrete embedded steel reinforcement. Cem. Concr. Res. **25**, 257–264 (1995). https://doi.org/10.1016/0008-8846(95)00006-2.
23. Ortega, J.M., Albaladejo, A., Pastor, J.L., Sánchez, I., Climent, M.A.: Influence of using slag cement on the microstructure and durability related properties of cement grouts for micropiles. Constr. Build. Mater. **38**, 84–93 (2013). https://doi.org/10.1016/j.conbuildmat.2012.08.036.
24. Mohammed, T.U., Hidennori, H., Toru, Y.: Performance of seawater-mixed concrete in the tidal environment. Cem. Concr. Res. 34, 593–601 (2004). https://doi.org/10.1016/j.cemconres.2003.09.020.
25. Li, P., Li, W., Sun, Z., Shen, L., Sheng, D.: Development of sustainable concrete incorporating seawater: A critical review on cement hydration, microstructure and mechanical strength. Cem. Concr. Compos. 121, 104100 (2021). https://doi.org/10.1016/j.cemconcomp.2021.104100.